Anisotropic x-ray magnetic linear dichroism at the Fe $L_{2,3}$ edges in Fe_3O_4

Elke Arenholz*
Advanced Light Source, Lawrence Berkeley National Laboratory, Berkeley, California 94720, USA

Gerrit van der Laan†
Magnetic Spectroscopy Group, Daresbury Laboratory, Warrington WA4 4AD, United Kingdom

Rajesh V. Chopdekar‡ and Yuri Suzuki
Department of Materials Science and Engineering, University of California-Berkeley, Berkeley, California 94720, USA
(Received 28 April 2006; revised manuscript received 27 June 2006; published 7 September 2006)

X-ray magnetic linear dichroism at the Fe $L_{2,3}$ edges of the ferrimagnet Fe_3O_4 was found to exhibit a strong dependence on the relative orientation of external magnetic field, x-ray polarization, and crystalline axes. Spectral shape and magnitude of the effect were determined for $Fe_3O_4(011)$ and $Fe_3O_4(001)$ thin films, varying the in-plane orientation of field and polarization. All dichroism spectra can be described as a linear combination of two fundamental spectra which in turn gives a good agreement with calculated spectra, using atomic multiplet theory. The angular dependence of the magnetic dichroism reflects the cubic crystal field symmetry. It can be used to estimate the crystal field splitting and allows the determination of the spin quantization axis.

DOI: 10.1103/PhysRevB.74.094407 PACS number(s): 75.50.Gg, 75.70.Ak, 78.20.Bh, 78.70.Dm

I. INTRODUCTION

Absorption spectroscopies utilizing synchrotron radiation have developed into important tools for the study of magnetic solids since the prediction and first observation of strong x-ray magnetic dichroism (XMD) at the $3d$ ($M_{4,5}$) edges of rare earth materials.[1,2] X-ray magnetic circular dichroism (XMCD) measures the difference in absorption of x rays with a helicity vector parallel and antiparallel to the magnetization direction. It is proportional to the average value $\langle \mathbf{M} \rangle$ of the local magnetic moment, so that ferromagnetic and ferrimagnetic order, but not antiferromagnetic order, can be probed. Its linear counterpart x-ray magnetic linear dichroism (XMLD) is the difference in absorption of linearly polarized x rays with polarization parallel and perpendicular to the magnetization direction. XMLD is assumed to be proportional to the square of the magnetic moment $\langle \mathbf{M}^2 \rangle$ and consequently, both ferromagnetically and antiferromagnetically ordered moments contribute to the XMLD signal. XMD is unique in its intrinsic element specificity[3] and chemical-site sensitivity[4] that allows the separation of the contributions of multiple magnetic species in alloys or layered systems.[5] Most importantly, theoretically derived sum rules link XMCD intensities to spin and orbital magnetic moments[6–8] and XMLD signals to the anisotropic spin-orbit moment which is directly proportional to magnetocrystalline anisotropy energy.[9,10] Sum rules enable the use of polarized x rays for quantitative magnetometry. Strong anisotropy in the XMLD has been reported both theoretically and experimentally.[11–14] Although magnetic spectroscopy techniques have found widespread use for the study of magnetic systems, the dependence of the XMLD signal on the relative orientation of external magnetic field, x-ray polarization, and crystalline axes has not been studied systematically to date. Together with the fact that in itinerant metallic ferromagnets the XMLD signal is much smaller than the XMCD effect, this might have hampered the development of XMLD to become an equally powerful probe as its circular counterpart.

The importance of structural or crystal field-induced linear dichroism has been studied for some time.[15–19] Instead we are concerned here with the interplay of crystal field and magnetization, which can lead to a rather complicated result. The geometrical aspects of the XMLD measurements have been largely ignored until recently, e.g., the Fe $L_{2,3}$ XMLD results of $CoFe_2O_4$ by Kuiper *et al.*[20] do not make any mention of measurement geometry.

In this paper, we present a systematic study of the influence of the geometry on the Fe $L_{2,3}$ XMLD in ferrimagnetic Fe_3O_4. Due to the localized nature of the magnetic moments in Fe_3O_4, the XMLD effects are much larger than in metallic ferromagnets. Also, due to its ferrimagnetic order, the magnetization can be rotated using external magnetic fields to allow a clear separation of magnetic and nonmagnetic contributions to the XMLD signal.[21] The Fe $L_{2,3}$ XMLD is found to exhibit a strong dependence on the relative orientation of external magnetic field, x-ray polarization, and crystal lattice, which can be used as a sensitive probe for the electronic and magnetic structure. We show that all XMLD spectra can be described as a linear combination of two fundamental spectra and that the angular dependence can be derived from atomic calculations based on the crystal-field symmetry.

II. EXPERIMENT

40 nm-thick Fe_3O_4 films were prepared on polished $SrTiO_3(011)$ and (001) substrates using pulsed laser deposition (PLD). The substrate was held at 725 K during sample preparation in an oxygen atmosphere of 10^{-6} Torr, leading to single crystalline films of proper stoichiometry. Exposure to air during sample transfer causes a slight change in surface stoichiometry which was quantified using XMCD and taken into account for the subsequent data analysis. Magneto-optical Kerr effect measurements showed that Fe_3O_4 films in compression on $SrTiO_3(011)$ exhibit an in-plane uniaxial an-

 ©2006 The American Physical Society

isotropy with easy magnetization axis along the [100] axis of the $SrTiO_3$ substrate and the Fe_3O_4 film. Grown on $SrTiO_3(001)$, the Fe_3O_4 films show a weak fourfold anisotropy with easy magnetization axes parallel to the [100] and [010] axes. At $T=298$ K, both films can be saturated along any in-plane direction by external magnetic fields of 0.5 T. The XMLD experiments were performed at beamline 4.0.2 at the Advanced Light Source[22] providing linearly polarized x rays with polarization direction continuously tunable through a 90° range and a degree of polarization of $(99\pm1)\%$. The eight-pole resistive magnet employed for these experiments allows applying magnetic fields up to 0.8 T in any direction.[23] All spectra were obtained by monitoring the sample drain current, i.e., in electron yield mode, in normal incidence at $T=298$ K in the presence of an external field of 0.5 T. The XMLD in three different geometries was measured by varying the orientation of external field, x-ray polarization, and sample orientation, respectively. To increase the electron-yield signal, the magnetic field was turned slightly out of the sample surface plane. Since this is a hard magnetic axis for the Fe_3O_4 samples studied here, the orientation of the magnetic moments is barely influenced by it. Varying the out-of-plane angle between 5° and 30° has no appreciable effect on the spectral shape and magnitude of the XMLD signal.

III. SYMMETRY CONSIDERATIONS

The geometrical properties of XMLD require more consideration than those for XMCD. The XMLD can be measured in a number of different ways, which calls for a transparent and concise notation. The XMLD is the difference between two x-ray absorption (XA) spectra measured with different orientations of **H** and **E** relative to the crystalline axes, where **E** is the linear polarization direction of the x rays and **H** the direction of the applied field. Usually, either **H** or **E** is rotated by 90° between the two successive XA measurements. We will choose the case that **H** and **E** are always in the plane of the surface, as this is the most practical experimental geometry.

To obtain the angular dependence of the XMLD, we rotate either **E**, **H** or the sample by an angle ϕ_E, ϕ_H, or ϕ_S, respectively, with respect to the [100] direction from 0° to 90° in the plane of the surface. This gives the XMLD signal in—what we will denote as—geometries 1, 2, and 3, respectively, defined as

$$I_{\mathrm{XMLD}}^{\mathrm{Geo.1}}(\phi_E) = I(\mathbf{H}_{0^\circ},\mathbf{E}_{\phi}) - I(\mathbf{H}_{90^\circ},\mathbf{E}_{\phi}), \tag{1}$$

$$I_{\mathrm{XMLD}}^{\mathrm{Geo.2}}(\phi_H) = I(\mathbf{H}_{\phi},\mathbf{E}_{0^\circ}) - I(\mathbf{H}_{\phi+90^\circ},\mathbf{E}_{0^\circ}), \tag{2}$$

$$I_{\mathrm{XMLD}}^{\mathrm{Geo.3}}(\phi_S) = I(\mathbf{H}_{\phi},\mathbf{E}_{\phi}) - I(\mathbf{H}_{\phi},\mathbf{E}_{\phi+90^\circ}), \tag{3}$$

where the subscripts of **E** and **H** indicate the angle of these vectors with respect to the [100] axis.

In geometry 1 [see inset to Fig. 1(a)] the two perpendicularly chosen **H** directions are fixed with respect to the sample. The XMLD is obtained as the difference of the XA spectra with **H** parallel and perpendicular to the [100] axis. The angular dependence of the XMLD is obtained by varying the angle ϕ_E between [100] and **E**.

In geometry 2 [see inset to Fig. 1(b)] **E** is fixed along the [100] axis of the sample. The XMLD is the difference of the XA spectra with **H** at angles ϕ_H and $\phi_H+90°$ with the [100] axis.

In geometry 3 [see inset to Fig. 1(c)] the sample is rotated about the surface normal, and the [100] axis is oriented at an angle ϕ_S relative to **H**. The XMLD is the difference of the XA spectra measured with horizontal and vertical linear polarization, i.e., with **E** parallel and perpendicular to **H**, respectively.

We studied two different surfaces, namely the (001) and (011) plane. The (001) plane has D_4 symmetry, which has a fourfold rotation axis and mirror planes at $\phi=0°$, 45°, and 90° normal to the surface. The (011) plane has D_2 symmetry, which has a twofold rotation axis and mirror planes at $\phi=0°$ and 90° normal to the surface. To justify our choice of these point group symmetries, we note that the (001) and (011) surfaces have C_{4v} and C_{2v} symmetry, respectively, which are isomorphic to the groups of pure rotations D_4 and D_2, respectively. The electron yield measurements have a probing depth of 2–5 nm, i.e., while relatively surface sensitive a substantial part of the signal comes from the bulk, where the (001) and (011) planes have D_4 and D_2 symmetry, respectively. In the case of XMLD, **H** and **E** can be considered as even (axial) vectors, which have D_2 symmetry in an orientation rotated about angles given by the subscripts in Eqs. (1)–(3). The angular dependence of the XMLD is subject to these symmetry properties. It will be useful to determine whether or not the angular dependence for each geometry is symmetric or antisymmetric with respect to $\phi=45°$. It is relative easy to verify that the symmetry properties lead to the following relations, given in Eqs. (4)–(6).

In geometry 1, for a plane with D_4 symmetry, a reflection of **E** with respect to $\phi_E=45°$ exchanges the two terms in Eq. (1), so that

$$I_{\mathrm{XMLD}}^{\mathrm{Geo.1}}(90^\circ - \phi_E) = -I_{\mathrm{XMLD}}^{\mathrm{Geo.1}}(\phi_E). \tag{4}$$

However, this does not hold for D_2 symmetry.

In geometry 2 for planes both of D_4 and D_2 symmetry, a reflection of **H** with respect to $\phi_H=45°$ exchanges the two terms in Eq. (2), so that

$$I_{\mathrm{XMLD}}^{\mathrm{Geo.2}}(90^\circ - \phi_H) = -I_{\mathrm{XMLD}}^{\mathrm{Geo.2}}(\phi_H). \tag{5}$$

In geometry 3 for a plane of D_4 symmetry, a reflection of both **H** and **E** with respect to $\phi_S=45°$ leaves each of the two terms in Eq. (3) invariant, so that

$$I_{\mathrm{XMLD}}^{\mathrm{Geo.3}}(90^\circ - \phi_S) = I_{\mathrm{XMLD}}^{\mathrm{Geo.3}}(\phi_S). \tag{6}$$

This does not hold for a D_2 symmetry.

Thus for the (001) plane in geometry 1 and 2 and for the (011) plane in geometry 2 the angular dependence is antisymmetric with respect to $\phi=45°$, and the XMLD spectra for ϕ and $90°-\phi$ have opposite signs, consequently the signal must vanish at $\phi=45°$. This behavior requires an angular dependence of the form $\cos 2\phi$.

For the (001) plane in geometry 3 the angular dependence is symmetric with respect to $\phi_S=45°$, and the XMLD for ϕ_S

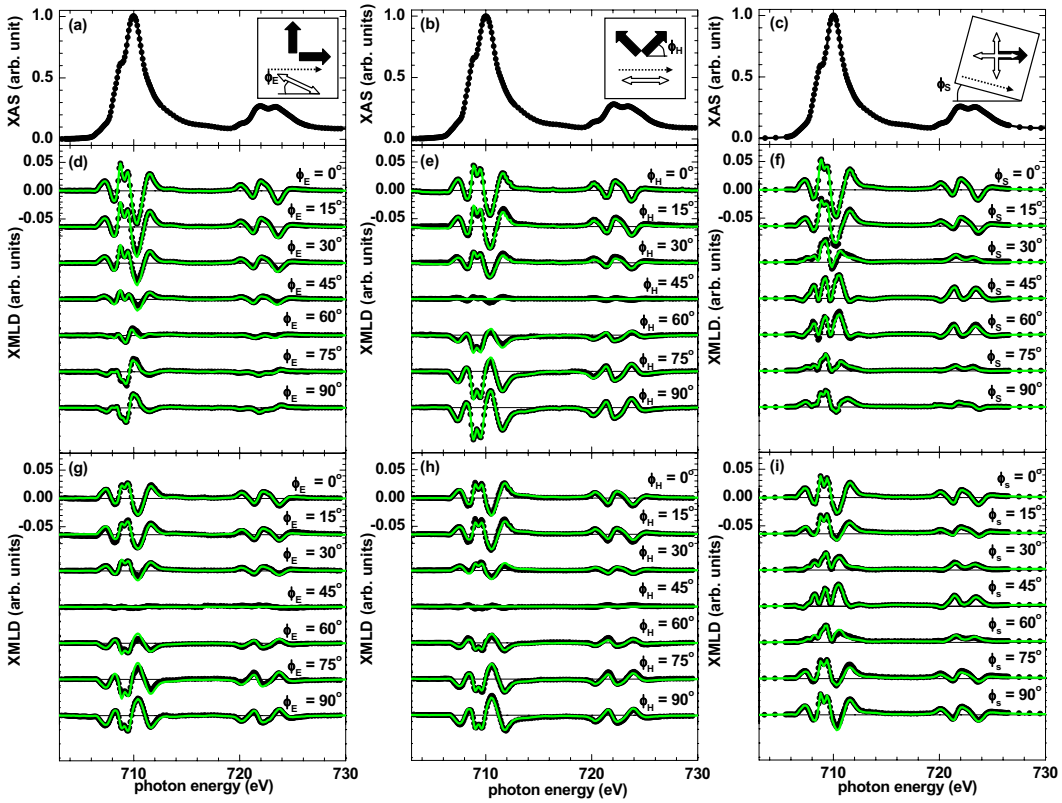

FIG. 1. (Color online) Angular dependence of the Fe $L_{2,3}$ XMLD in $Fe_3O_4/SrTiO_3(011)$ and $Fe_3O_4/SrTiO_3(001)$. Experimental XMLD spectra obtained for three geometries 1, 2, and 3, varying the relative orientation of external field, x-ray polarization, and sample orientation, respectively, are shown in the left, center, and right panels, respectively. Top panels (a), (b), and (c) show XA spectra averaged over all azimuthal angles measured in one geometry. The insets in panels (a), (b), and (c) depict the experimental geometries [cf. Eqs. (1)–(3)] with black arrows indicating the orientation of the external magnetic fields, white arrows the polarization of the linearly polarized x rays, and dashed arrows the [100] easy magnetization axis. The center panels (d), (e), and (f) show XMLD spectra obtained from $Fe_3O_4/SrTiO_3(011)$, whereas (g), (h), and (i) show results for $Fe_3O_4/SrTiO_3(001)$ at $T=298$ K. Experimental data are represented by solid symbols and results of the modeled angular dependence by lines.

and $90°-\phi_S$ have the same sign and hence does not vanish at $\phi_S=45°$ (unless accidentally). This behavior requires a $\cos 4\phi_S$ term in the angular dependence.

The angular dependence of the XMLD can be written in terms of three spectra I_0, I_{45}, and I_{90}, which are the XMLD spectra for $\phi=0°$, 45°, and 90° in the given geometry. The expressions can be derived from the symmetry properties given in Eqs. (4)–(6), considering the following principles. In all cases the angular dependence is symmetric with respect to $\phi=0°$ and 90°, thus it must consist of terms $\cos 2n\phi$, where n is an integer. The term $\cos 2\phi$ gives an angular dependence that is antisymmetric with respect to $\phi=45°$. The term $\cos 4\phi$ gives an angular dependence that is symmetric with respect to $\phi=45°$. Higher-order terms are ignored. The coefficient of the $\cos 2n\phi$ term is determined by the difference between the spectra at angles where the cosine is ±1. Furthermore, there is a constant term present, if the average over the different angles does not cancel.

In geometry 1, according to Eq. (4) the angular dependence is asymmetric with respect to $\phi=45°$ for D_4 symmetry. This means that in the case of the broken symmetry (i.e., D_2 symmetry) of the (011) plane there is a constant term equal to $\frac{1}{2}(I_0+I_{90})$ in addition to the angular dependent $\cos 2\phi$ term with coefficient $\frac{1}{2}(I_0-I_{90})$, so that

$$I^{\text{Geo.1}}_{\text{XMLD}(011)}(\phi_E) = \tfrac{1}{2}(I_0+I_{90}) + \tfrac{1}{2}(I_0-I_{90})\cos 2\phi_E = I_0\cos^2\phi_E + I_{90}\sin^2\phi_E. \quad (7)$$

For the (001) plane in geometry 1, the angular dependence in Eq. (7) simplifies by substitution of $I_{90}=-I_0$, resulting in

$$I^{\text{Geo.1}}_{\text{XMLD}(001)}(\phi_E) = I_0\cos 2\phi_E = I_0(\cos^2\phi_E - \sin^2\phi_E), \quad (8)$$

where as anticipated the constant term drops out.

In geometry 2, according to Eq. (5) the angular dependence is antisymmetric with respect to $\phi=45°$ for both the (011) and (001) plane and we have $I_{90}=-I_0$, so that

$$I^{\text{Geo.2}}_{\text{XMLD}}(\phi_H) = I_0\cos 2\phi_H = I_0(\cos^2\phi_H - \sin^2\phi_H). \quad (9)$$

In geometry 3, for the (011) plane the angular dependence of the XMLD is given as

$$\begin{aligned} I^{\text{Geo.3}}_{\text{XMLD}(011)}(\phi_S) &= \tfrac{1}{4}(I_0+2I_{45}+I_{90}) + \tfrac{1}{2}(I_0-I_{90})\cos 2\phi_S \\ &\quad + \tfrac{1}{4}(I_0-2I_{45}+I_{90})\cos 4\phi_S \\ &= I_0(\cos^4\phi_S - \cos^2\phi_S\sin^2\phi_S) \\ &\quad + 4I_{45}\cos^2\phi_S\sin^2\phi_S \\ &\quad + I_{90}(\sin^4\phi_S - \cos^2\phi_S\sin^2\phi_S). \end{aligned} \quad (10)$$

For the (001) plane in geometry 3, the angular dependence simplifies with $I_{90}=I_0$, resulting in

$$I^{\text{Geo.3}}_{\text{XMLD}(001)}(\phi_S) = \tfrac{1}{2}(I_0 + I_{45}) + \tfrac{1}{2}(I_0 - I_{45})\cos 4\phi_S = I_0(\cos^2\phi_S - \sin^2\phi_S)^2 + 4I_{45}\cos^2\phi_S \sin^2\phi_S. \quad (11)$$

For convenience we have also included in Eqs. (7)–(11) the expressions in terms of $\cos^2\phi$ and $\sin^2\phi$, which can sometimes provide a better visualization of the angular dependence.

We now come to the important point of the number of fundamental spectra, i.e., the minimum number of spectra required to generate all other spectra by making linear combinations of the former. From the above symmetry arguments within a given measurement plane this number seems to be equal to three. However, in cubic symmetry there is an extra condition due to the fact that the directions $\phi=45°$ in the (001) plane and $\phi=90°$ in the (011) plane are equivalent since they both represent ⟨110⟩ directions. Using this extra symmetry requirement it is possible to show that $I_{90}=\frac{1}{2}(I_0+I_{45})$ for the (011) plane in geometry 3 and furthermore $I_{90}(\text{Geo.1})=-I_{90}(\text{Geo.3})$. These conditions can be substituted in Eqs. (10) and (7), respectively, eliminating I_{90}. Thus we can conclude that in cubic symmetry there are only two fundamental spectra, namely I_0 and I_{45}. We define the latter fundamental spectrum as being equal to I_{45}(Geo.3), which is the same for both (001) and (011) planes.

IV. RESULTS

XMLD spectra obtained in geometries 1, 2, and 3 for $Fe_3O_4/SrTiO_3(011)$ and $Fe_3O_4/SrTiO_3(001)$ are plotted in the left, center, and right panels of Fig. 1, respectively. The top panels (a), (b), and (c) show the XA spectra obtained by averaging over all azimuthal angles measured in each geometry. The center panels (d), (e), and (f) show XMLD spectra obtained from $Fe_3O_4/SrTiO_3(011)$ and the bottom panels (g), (h), and (i) show results for $Fe_3O_4/SrTiO_3(001)$.

For all three geometries, the experimental XMLD spectra for $Fe_3O_4/SrTiO_3(011)$ and $Fe_3O_4/SrTiO_3(001)$ show pronounced variations in the XMLD spectral shape and magnitude with ϕ, but differences between the two samples clearly exist. So the XMLD spectra for $\phi_E=0°$ and $\phi_E=90°$ show significant differences in the case of $Fe_3O_4/SrTiO_3(011)$ [cf. Fig. 1(d)] whereas for $Fe_3O_4/SrTiO_3(001)$ [cf Fig. 1(g)] they only differ in their sign.

To test the validity of the predicted angular dependence of the XMLD signal, XMLD spectra were modeled employing Eqs. (7)–(11) using experimental data for the fundamental spectra. The lines in Fig. 1 indicate the results of this approach. The agreement with the experimental data is good for both samples. The XMLD signal should vanish completely at $\phi_E=45°$ for $Fe_3O_4/SrTiO_3(001)$ in geometry 1 and for both samples at $\phi_H=45°$ in geometry 2. While indeed within the experimental accuracy no XMLD is observed at $\phi_E=45°$ for $Fe_3O_4/SrTiO_3(001)$ in geometry 1; the small residual XMLD found in geometry 2 is the consequence of a 2° misalignment between external magnetic field and polarization vector.

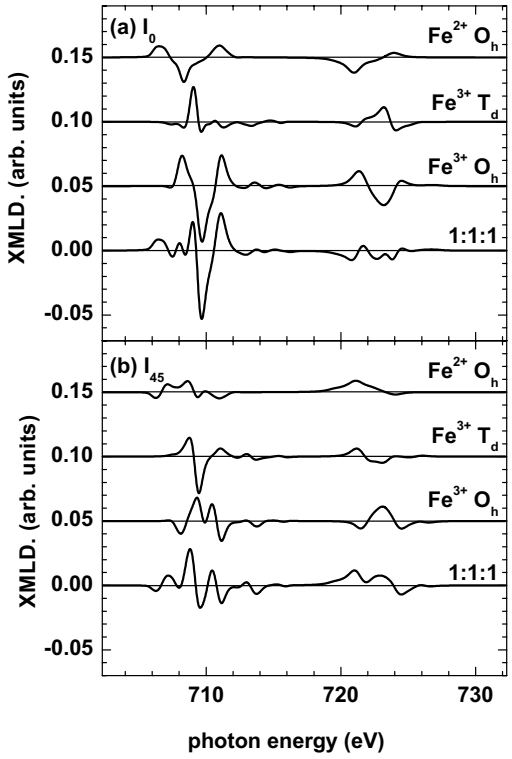

FIG. 2. The calculated XMLD spectra for the three different sites Fe^{2+} O_h, Fe^{3+} T_d, and Fe^{3+} O_h together with the summed spectrum for the stoichiometric 1:1:1 ratio. (a) I_0 and (b) I_{45}.

V. CALCULATIONS

The XMLD spectra are compared with atomic multiplet calculations. We recall that Fe_3O_4 has an inverse spinel-type structure.[24] Half of the Fe^{3+} ions are tetrahedrally coordinated (T_d) whereas the remaining Fe^{3+} ions, as well as the Fe^{2+} ions, occupy octahedrally coordinated sites (O_h). The magnetic moments on T_d and O_h sites are coupled antiferromagnetically.

Figure 2 shows the calculated XMLD spectra for the three different sites Fe^{2+} d^6 O_h, Fe^{3+} d^5 T_d, and Fe^{3+} d^5 O_h. The calculational method follows that of Ref. 25. The $L_{2,3}$ XA spectra with **H** and **E** along specified directions were obtained from the electric-dipole allowed transitions between the ground state $3d^n$ and the final state $2p^5 3d^{n+1}$ configuration. The wave functions of ground and final states were calculated at a temperature $T=0$ in intermediate coupling using Cowan's Hartree-Fock code with relativistic correction.[26] The Slater and spin-orbit parameters are as tabulated in Ref. 27. Interatomic screening and mixing was taken into account by reducing the *d-d* and *p-d* Slater integrals with scaling factors of 0.7 and 0.8, respectively. For the octahedral site a crystal field of $10Dq=1.2$ eV and exchange field of $g\mu_B H=0.01$ eV were used. For the tetrahedral site a crystal field of $10Dq=-0.6$ eV and exchange field of $g\mu_B H=-0.01$ eV was used. The calculated results were broadened by a Lorentzian of $\Gamma=0.3(0.5)$ eV for the L_3 (L_2) edge to account for intrinsic linewidth broadening and a Gaussian of $\sigma=0.25$ eV for the instrumental broadening. The relative-energy positions of the spectra for the three different

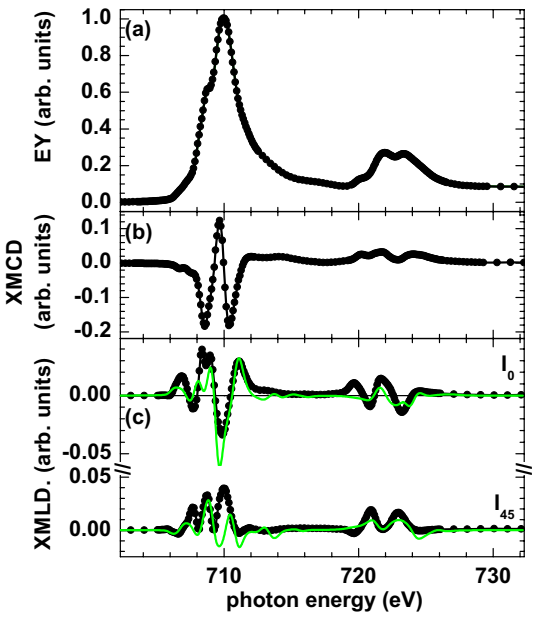

FIG. 3. (Color online) (a) Fe $L_{2,3}$ XA spectrum from Fe_3O_4. (b) The corresponding XMCD spectrum obtained in normal incidence. (c) The experimental XMLD spectra I_0 and I_{45} (dots) compared to the calculated spectra (green line) at $\phi=0°$ from Figs. 1(d)–1(i) and $\phi_S=45°$ in Fig. 1(f) and 1(i). In the calculation an Fe^{2+} O_h: Fe^{3+} T_d: Fe^{3+} O_h ratio of 0.8:1:1.2 is assumed, as obtained from the XMLD spectrum (see text).

Fe sites were taken as obtained previously for the XMCD of Fe_3O_4.[28] Figure 2 shows also the sum spectra with the stoichiometric ratio 1:1:1 for the different Fe sites. It will be clear that due to the spectral complexity with the large amount of nodes (zero crossings) of the individual XMLD spectra, a small shift in the relative energy positions for the three different sites can give a large change in the sum spectrum.

VI. COMPARISON TO EXPERIMENT

Magnetite samples can be notoriously nonstoichiometric. Sample exposure to atmosphere during sample transfer from the preparation chamber to the magnet chamber can change the sample stoichiometry near the surface region. A sensitive method to determine the stoichiometry of the sample is offered by the XMCD that can be measured in combination with the XMLD. We determined the relative concentrations of the three Fe sites by fitting the three peaks in the measured L_3 XMCD. This is a well-established method that has been tested on a wide variety of spinel ferrites.[28] The relative peak intensities can be calibrated to those for the stoichiometric ratio as reported by Morrall *et al.*[4] for a 24 ML Fe_3O_4 film grown on Pt(111), Pellegrin *et al.*,[29] and Chen *et al.*[30] for a thin film of magnetite on MgO(001).

The Fe_3O_4 XA spectrum is plotted in Fig. 3(a) and the measured XMCD averaged over all angles is shown in Fig. 3(b). We find only a very small angular dependence in the XMCD, which is in agreement with previous findings by Edmonds *et al.*[31] for Mn d^5 in (Ga,Mn)As. From the XMCD measurement we obtain an Fe^{2+} O_h: Fe^{3+} T_d: Fe^{3+} O_h ratio of 0.8:1:1.2. We use these weighting factors to correct the calculated XMLD. The result is shown in Fig. 3(c) and compared to the experimental I_0 spectrum [$\phi=0°$ from Figs. 1(d)–1(i)] and I_{45} spectrum [$\phi_S=45°$ from Figs. 1(f) and 1(i)]. Comparing the I_0 and the I_{45} spectrum to each other, one observes roughly a tendency for the signal to reverse sign, however, the detailed multiplet structure is much more complicated and is not following a simple pattern.

We observe a good agreement between the experimental and calculated spectra in Fig. 3(c). However, that is not to say that there would not be any room for improvement. The valence on the octahedral sites is on average 2.5+ and full charge separation would mean equal amounts of sites being 2+ and 3+. Several recent diffraction experiments[32–34] have suggested that the charge difference might be much smaller than one electron, probably 0.2–0.3 electron. Although multiplet structures can be calculated for noninteger valence charges, it allows for additional fitting parameters, which makes the results less clear cut than for integer valence charges. Noninteger charges on each site can be included by taking charge-transfer into account, where the local ground state at each site is a mixture of different configurations d^n and $d^{n+1}\underline{L}$, with the underscore denoting a hole on a ligand oxygen site.[35] The ground and final states now depend on the d-$\underline{L}$ charge transfer energy, the d-d on-site Coulomb interaction and the d-$\underline{L}$ mixing (hybridization). Since the core hole in the XA process is well screened by the electron excited into the d band, the change in hybridization upon core-hole creation will be small, which results in only weak charge-transfer satellite structure in the XA spectra that can be present at the high energy tail above each edge. A second effect of the charge-transfer is a reduction in overall width of the multiplet structure, which can approximately be taken into account by a reduction of the Slater integrals.[35] Hence for the XA spectra reasonable agreement can often be obtained by describing the measured spectra using configurations with integer charges. However, it would be interesting to see how sensitive the spectral shape would be in the case of XMLD. In the first instance one might expect that the spectral shapes for Fe^{2+} d^6 O_h and Fe^{3+} d^5 O_h would become more similar if there is significant hybridization between the two octahedral sites. As a consequence the large negative peak in the I_0 spectrum in Fig. 2(a) would reduce in magnitude.

Sum rules give the relation between the integrated intensities $A_{2,3}$ of the $L_{2,3}$ XMLD spectra and the expectation values of ground-state operators. The integrals A_3+A_2 and A_3-2A_2 are proportional to the charge quadrupole moment and the anisotropic spin-orbit interaction, respectively.[21] In second-order perturbation theory, the latter is related to the magnetocrystalline anisotropy energy (MAE).[21] The integral A_3-2A_2 is usually small compared to the intensities of the individual peaks in the XMLD, and therefore difficult to measure unless the MAE is large.[10,36] For high spin Fe d^5 in cubic symmetry, with its half-filled shell, the charge quadrupole and the MAE are essentially zero, however, as seen in Fig. 2, the anisotropy in the XMLD for d^5 is as strong as for d^6, if not stronger. So do the spectral features in I_0 and I_{45} at 708.5 eV and 721 eV have an opposite sign for Fe^{2+} d^6 O_h

similarly to features near 709 eV and 723 eV for Fe^{3+} d^5 T_d, whereas a vanishing XMLD anisotropy would obviously manifest itself in identical I_0 and I_{45} spectra. It is clear that the large angular dependence of the XMLD for d^5 with a half-filled shell and vanishing spin-orbit splitting cannot be ascribed to a large MAE.

In fact, the origin of the anisotropic XMLD has a more complicated reason. It stems from the electric-dipole selection rules restricting the set of final states that can be reached from the ground state. This can be seen, e.g., in geometry 1 by substituting Eq. (1) into Eq. (7), which gives

$$I_{\mathrm{XMLD}}^{\mathrm{Geo.1}}(\phi_E) = [I_{\mathrm{XA}}(\mathbf{H}_0,\mathbf{E}_0) - I_{\mathrm{XA}}(\mathbf{H}_{90},\mathbf{E}_0)]\cos^2\phi_E + [I_{\mathrm{XA}}(\mathbf{H}_0,\mathbf{E}_{90}) - I_{\mathrm{XA}}(\mathbf{H}_{90},\mathbf{E}_{90})]\sin^2\phi_E. \tag{12}$$

Here, $I_{\mathrm{XA}}(\mathbf{H}_0,\mathbf{E}_0)$ and $I_{\mathrm{XA}}(\mathbf{H}_{90},\mathbf{E}_{90})$ are the XA spectra for transitions $\Delta m=0$ with the quantization axis along $\phi=0°$ and 90°, respectively. $I_{\mathrm{XA}}(\mathbf{H}_{90},\mathbf{E}_0)$ and $I_{\mathrm{XA}}(\mathbf{H}_0,\mathbf{E}_{90})$ are the XA spectra for transitions $\Delta m=\pm 1$ with the quantization axis along $\phi=90°$ and 0°, respectively. This gives different transition probabilities from the exchange-split core levels to the t_2 and e crystal-field-split empty d states. Therefore, the strong angular dependence is a property of the cubic wave functions for the d states with respect to the spin quantization axis. Hence, the angular dependence disappears when the crystal-field splitting goes to zero. The angular dependent XMLD allows determining the spin quantization axis with respect to the crystalline axes and can be used to estimate the crystal-field splitting. The effect in the other two geometries is similar. In geometry 3, rotation of the sample and the consequent rotation of the d states, give new functions t_2' and e' that are linear combinations of functions t_2 and e, hence changes the transition probabilities in the XMLD.

VII. CONCLUSIONS

We have performed a comprehensive XMLD study in three different geometries for two separate crystal planes in Fe_3O_4. The results evidence the presence of a strong angular dependence in the XMLD across the Fe $L_{2,3}$ edges. The angular dependence can be understood from the cubic symmetry of the crystal structure, where the symmetry properties allow condensing the spectral information into two fundamental spectra.

Even in the case of the half-filled shell of the high spin Fe d^5 configuration in cubic symmetry, where the charge quadrupole moment and anisotropic spin-orbit interaction are zero, the XMLD shows a large angular dependence. Therefore, this angular dependence should not be ascribed to the MAE. Instead, the angular dependence is a property of the cubic wave functions for the d valence states with respect to the spin quantization axis. The anisotropic XMLD can be used to estimate the crystal-field splitting and allows determining the spin quantization axis with respect to the crystalline axes. The usefulness of the latter has already been demonstrated in the case of photoelectron emission microscopy (PEEM) studies with linearly polarized light.[13] Interesting applications might emerge in cases where the spin axis rotates, such as in domain switching, hysteresis curve, and magnetostriction measurements, as well as in systems with noncollinear or canted spins in, e.g., magnetic thin films and surfaces.

Our study shows that the anisotropy of the dichroism should be taken into account in all XMLD studies. This should not only be done in measurements on single crystals but also for randomly oriented samples, since the XMLD spectrum is determined by the orientation of **H** and **E** with respect to the crystalline axes. It should also be clear that one has to be careful using XMLD as a magnetometer to measure $\langle \mathbf{M}^2 \rangle$. Such measurements are possible but require fixed geometry and crystal orientation. There are even certain orientations, such as in geometries 1 and 2 along [110] in the (001) plane, where the XMLD completely disappears, whereas it does not disappear along the same [110] direction in the (011) plane. We have given simple symmetry rules to predict orientations where the XMLD vanishes.

The observed anisotropy in the XMLD is in good agreement with atomic multiplet calculations in cubic crystal field. The spectral structure is very rich and quite sensitive to small changes in the chemical shift and hybridization of the different Fe sites. Therefore, combined with model calculations, XMLD has the potential to become an important tool to monitor small changes in the electronic and magnetic structure of magnetic materials. The case of Fe_3O_4, for which the charge and spin density on the different sites is still a matter of debate, is in this respect a rather complicated example, which requires further theoretical study.

In our approach we have separated the XMLD results in a part that depends on the physics (dynamics) and a part that depends on the geometry. The former is described by the fundamental spectra and will sensitively depend on the electronic structure and composition of the material, as well as on external parameters such as the temperature. These spectra need to be calculated using a suitable model such as multiplet theory or band-structure theory. Despite the good agreement with theoretical results, it has not been the aim of the current paper to offer a final answer regarding the complex nature of the Fe_3O_4 spectra. The geometrical part, on the other hand, depends on the symmetry of the crystal and the relative orientations of the magnetic field and the light polarization. This part leads to specific rules that can be considered to be valid within the assumptions made concerning the geometry. Hence the conclusions that arise from the symmetry arguments should be valid beyond the model calculations used to reproduce the spectral shape of the fundamental spectra.

ACKNOWLEDGMENTS

The Advanced Light Source is supported by the Director, Office of Science, Office of Basic Energy Sciences, of the U.S. Department of Energy under Contract No. DE-AC02-05CH11231.

*Electronic address: earenholz@lbl.gov
†Electronic address: g.vanderlaan@dl.ac.uk
‡Also at School of Applied Physics, Cornell University, Ithaca, NY 14853.

[1] B. T. Thole, G. van der Laan, and G. A. Sawatzky, Phys. Rev. Lett. **55**, 2086 (1985).
[2] G. van der Laan, B. T. Thole, G. A. Sawatzky, J. B. Goedkoop, J. C. Fuggle, J.-M. Esteva, R. Karnatak, J. P. Remeika, and H. A. Dabkowska, Phys. Rev. B **34**, 6529 (1986).
[3] Y. U. Idzerda, L. H. Tjeng, H.-J. Lin, C. J. Gutierrez, G. Meigs, and C. T. Chen, Phys. Rev. B **48**, 4144 (1993).
[4] P. Morrall, F. Schedin, G. S. Case, M. F. Thomas, E. Dudzik, G. van der Laan, and G. Thornton, Phys. Rev. B **67**, 214408 (2003).
[5] M. G. Samant, J. Stohr, S. S. P. Parkin, G. A. Held, B. D. Hermsmeier, F. Herman, M. V. Schilfgaarde, L. C. Duda, D. C. Mancini, N. Wassdahl, and R. Nakajma, Phys. Rev. Lett. **72**, 1112 (1994).
[6] B. T. Thole, P. Carra, F. Sette, and G. van der Laan, Phys. Rev. Lett. **68**, 1943 (1992).
[7] P. Carra, B. T. Thole, M. Altarelli, and X. Wang, Phys. Rev. Lett. **70**, 694 (1993).
[8] C. T. Chen, Y. U. Idzerda, H.-J. Lin, N. V. Smith, G. Meigs, E. Chaban, G. H. Ho, E. Pellegrin, and F. Sette, Phys. Rev. Lett. **75**, 152 (1995).
[9] G. van der Laan, Phys. Rev. Lett. **82**, 640 (1999).
[10] S. S. Dhesi, G. van der Laan, E. Dudzik, and A. B. Shick, Phys. Rev. Lett. **87**, 067201 (2001).
[11] G. van der Laan, Phys. Rev. B **57**, 5250 (1998).
[12] J. Kuneš and P. M. Oppeneer, Phys. Rev. B **67**, 024431 (2003).
[13] S. Czekaj, F. Nolting, L. J. Heyderman, P. R. Willmott, and G. van der Laan, Phys. Rev. B **73**, 020401(R) (2006).
[14] A. A. Freeman, K. W. Edmonds, G. van der Laan, N. R. S. Farley, T. K. Johal, E. Arenholz, R. P. Campion, C. T. Foxon, and B. L. Gallagher, Phys. Rev. B **73**, 233303 (2006).
[15] B. T. Thole, G. van der Laan, and P. H. Butler, Chem. Phys. Lett. **149**, 295 (1988).
[16] C. Brouder, J. Phys.: Condens. Matter **2**, 701 (1990).
[17] M. Sacchi, O. Sakho, and G. Rossi, Phys. Rev. B **43**, 1276 (1991).
[18] G. van der Laan, P. F. Schofield, G. Cressey, and C. M. B. Henderson, Chem. Phys. Lett. **252**, 272 (1996).
[19] M. W. Haverkort, S. I. Csiszar, Z. Hu, S. Altieri, A. Tanaka, H. H. Hsieh, H.-J. Lin, C. T. Chen, T. Hibma, and L. H. Tjeng, Phys. Rev. B **69**, 020408(R) (2004).
[20] P. Kuiper, B. G. Searle, L.-C. Duda, R. M. Wolf, and P. van der Zaag, J. Electron Spectrosc. Relat. Phenom. **86**, 107 (1997).
[21] G. van der Laan, Phys. Rev. Lett. **82**, 640 (1999).
[22] A. T. Young, E. Arenholz, S. Marks, R. Schlueter, C. Steier, H. A. Padmore, A. P. Hitchcock, and D. G. Castner, J. Synchrotron Radiat. **9**, 270 (2002).
[23] E. Arenholz and S. O. Prestemon, Rev. Sci. Instrum. **76**, 083908 (2005).
[24] J. Smit and H. P. J. Wijn, *Ferrites. Physical properties of ferrimagnetic oxides in relation to their technical applications.* (Wiley, New York, 1959).
[25] G. van der Laan and B. T. Thole, Phys. Rev. B **43**, 13401 (1991).
[26] R. D. Cowan, *The Theory of Atomic Structure and Spectra* (University of California Press, Berkeley, 1982).
[27] G. van der Laan and I. W. Kirkman, J. Phys.: Condens. Matter **4**, 4189 (1992).
[28] R. A. D. Pattrick, G. van der Laan, C. M. B. Henderson, P. Kuiper, E. Dudzik, and D. J. Vaughan, Eur. J. Mineral. **14**, 1095 (2002).
[29] E. Pellegrin, M. Hagelstein, S. Doyle, H. O. Moser, J. Fuchs, D. Vollath, S. Schuppler, M. A. James, S. S. Saxena, L. Niesen, *et al.*, Phys. Status Solidi B **215**, 797 (1999).
[30] J. Chen, D. J. Huang, A. Tanaka, C. F. Chang, S. C. Chung, W. B. Wu, and C. T. Chen, Phys. Rev. B **69**, 085107 (2004).
[31] K. W. Edmonds, G. van der Laan, A. Freeman, N. R. S. Farley, T. K. Johal, R. P. Campion, C. T. Foxon, B. L. Gallagher, and E. Arenholz, Phys. Rev. Lett. **96**, 117207 (2006).
[32] J. P. Wright, J. P. Attfield, and P. G. Radaelli, Phys. Rev. B **66**, 214422 (2002).
[33] R. J. Goff, J. P. Wright, J. P. Attfield, and P. G. Radaelli, J. Phys.: Condens. Matter **17**, 7633 (2005).
[34] E. Nazarenko, J. E. Lorenzo, Y. Joly, J. L. Hodeau, D. Mannix, and C. Marin, Phys. Rev. Lett. **97**, 056403 (2006).
[35] G. van der Laan, J. Zaanen, G. A. Sawatzky, R. Karnatak, and J.-M. Esteva, Phys. Rev. B **33**, 4253 (1986).
[36] S. S. Dhesi, G. van der Laan, and E. Dudzik, Appl. Phys. Lett. **84**, 2661 (2004).